

## ■ ORIGINAL PAPER ■

## Some Ingenious Techniques for Imaging Multiphase Processes of Micro Plastic Resin Particles under Abrupt Heating

OHIWA, Norio<sup>1\*</sup>, ISHINO, Yojiro<sup>1</sup>, and YAMAKITA, Ryuji<sup>2</sup>

<sup>1</sup> Nagoya Institute of Technology, Gokiso-cho, Showa-ku, Nagoya 466-8555, Japan

<sup>2</sup> Technical Company, Ishizuka Glass Co. Ltd., 1880 Kawai-cho, Iwakura 482-8510, Japan

Received 7 September, 2007; Accepted 26 October, 2007

**Abstract** : In order to observe and elucidate multiphase process of micro plastic resin particles under abrupt heating, some ingenious techniques are devised and introduced in this investigation; two devises for optical imaging and four devises for abrupt heating and extinguishment. One of the two optical devises is a mini optical composite which enables simultaneous photographing of direct silhouetted image and schlieren image, and another is a magnifying particle tracking system which realizes a wide and straight tracking range up to about 50 mm. In the latter four devises, on the other hand, reforming of a ragged resin particle into a spherical one around a fine tungsten wire of 5  $\mu\text{m}$  diameter, a vertical type cylindrical mini burner for abrupt heating, a mini-puff generator for abrupt extinguishment of all flames around a PET particle at an arbitrary assigned time after the abrupt heating, and a slot burner having extremely fine two-dimensionality are introduced. According to various optical observations using these devised techniques, many characteristic behaviors, such as occurrence of internal multiple micro bubbling, micro explosions and jets, and transformation of a slender wake flame into a long and thin cluster consisting of multiple micro brilliant spots within a short passage about a few millimeters, are clarified with respect to multiphase process of plastic resin particles under abrupt heating.

**Key Words** : Combustion, Optical imaging technique, Plastic resin particle, Thermal decomposition, Gasification, Micro bubbling, Micro explosion

### 1. Introduction

The possibility and availability of thermal recycling of waste plastic resin have been investigated experimentally by supplying plastic resin powder as an additional fuel to a proposed twin-fueled industrial burner [1, 3, 4, 6-8, 10]. The preceding experimental investigations have emphasized the necessity of fundamental investigations, such as high-speed microscopic or magnifying optical observation of multiphase processes of micro plastic particles under abrupt heating. High temperature combustion gas behind a premixed laminar flame is used as a heat source, to simulate the real situation which plastic resin powder experiences during its passage through the combustion zone in the industrial burner.

Two sets of optical imaging systems are devised in this investigation; one is for high-speed simultaneous observation of direct and schlieren images around a micro plastic particle under abrupt heating [2, 5, 9], the other is for high-speed and magnifying tracking of micro plastic particles passing through

a premixed flame sheet [11]. Four devises are also introduced for abrupt heating and extinguishment of micro plastic particles. For abrupt heating of a micro plastic particle, an original ragged particle is first reformed into a spherical one having a diameter of about 200  $\mu\text{m}$ , not only to improve the accuracy and reproducibility of data acquisition but also to solve the problem how to support surely a micro plastic particle [2]. A vertical type cylindrical mini-burner and a mini-puff generator are used for abrupt heating and abrupt extinguishment, respectively. For high-speed magnifying tracking of micro plastic particles flying through a flame sheet, a laminar premixed slot burner exhibiting extremely fine two-dimensionality and a transparent side view is constructed to obtain clear images of plastic particles passing through the flame sheet [11]. These devised techniques are summarized in Table 1, where a suitable combination for each optical imaging is also shown. For imaging the abrupt heating process of a micro plastic particle, a mini schlieren system, plastic particle reforming, a cylindrical mini-burner and a mini-puff generator are used, whereas for magnifying tracking of micro plastic particles a rotating mirror system and a slot burner are combined with each other.

\* Corresponding author. E-mail: oiwa.norio@nitech.ac.jp

Table 1 Optical and heating devises introduced in this investigation and suitable combination in each optical imaging

	Optical devises		Heating and extinguishment devises			
	Mini schlieren system	Rotating mirror system	Reforming of plastic particle	Cylindrical mini-burner	Mini-puff generator	Slot burner
Abrupt heating of a micro PET particle	○	—	○	○	○	—
Magnifying tracking of PET particles	—	○	—	—	—	○

Polyethylene terephthalate resin, abbreviated to PET-resin in the following, is used as solid particles, since it is the most familiar plastic resin used for a wide variety of containers and, therefore, a great deal of PET bottles and containers has been wasted and accumulated. PET-resin is one of the oxygenated polyesters and is also characterized by its unique chemical composition containing not only benzene nucleus but also char at about 17 wt % [12-15]. In this paper PET powder having a median diameter of  $d_m = 176.4 \mu\text{m}$  is used as micro plastic particles. High-speed direct and schlieren images of a spherical PET particle under abrupt heating and high-speed magnifying tracking images of PET particles flying through a premixed flame sheet are collected using the two types of proposed optical systems. According to detailed analysis of various imaging data, many interesting and characteristic behaviors can be observed with respect to the physical and chemical processes of PET particle under abrupt heating, and some of the key factors to intense thermal decomposition and gasification of plastic resin particles are qualitatively clarified in this paper.

## 2. Nomenclature

$C_b$	: burning rate constant, $\text{mm}^2/\text{s}$
$d$	: PET particle diameter, $\mu\text{m}$
$d_0$	: initial diameter of PET particle, $\mu\text{m}$
$d_m$	: median diameter of PET-powder, $\mu\text{m}$
$m_{\text{PET}}$	: mass flow rate of PET-powder, $\text{g}/\text{min}$
PET	: polyethylene terephthalate
$q_3$	: mass-based fraction in the histogram, %
$S_u$	: laminar burning velocity, $\text{m}/\text{s}$
$T_f$	: combustion gas temperature, $\text{K}$
$T_g$	: heating temperature, $\text{K}$
$t$	: heating time after the abrupt heating, $\text{ms}$
$u'$	: fluctuation velocity in the axial direction, $\text{m}/\text{s}$
$U$	: mean velocity of propane-air mixture, $\text{m}/\text{s}$
$x, y, z$	: rectangular coordinate system taken at the burner exit, where $z$ presents the axial distance, $\text{mm}$
$\Delta y$	: deviation in the direction to the depth, $\text{mm}$
$\Delta z$	: tracking distance in the axial direction, $\text{mm}$

## Greek Symbols

$\phi$	: equivalence ratio of propane-air mixture
$\tau$	: blow-off timing after the abrupt heating, $\text{ms}$
$\omega_1, \omega_2$	: angular velocity of Mirror 1 and 2, respectively, $\text{rad}/\text{s}$

## 3. Experimental Apparatus and Methods

The schematic arrangements of the two proposed sets of imaging systems are separately explained in the following as “simultaneous high-speed direct and schlieren system” and “high-speed magnifying and tracking system”.

### 3.1. Simultaneous High-speed Direct and Schlieren System

The schematic diagram of the simultaneous high-speed direct and schlieren system for the abrupt heating experiment of a micro PET particle is presented in Fig. 1. The system is composed of a propane supply line, an air supply line, a mini-burner for abrupt heating, a mini schlieren optical system and a high-speed CCD video camera. The following three devices are introduced in this system; a high-speed microscopic direct and schlieren system, a premixed mini-burner for abrupt heating, and a single mini-puff generator to cease heating and combustion instantaneously.

The arrangement of the straight type mini schlieren system is presented in Fig. 2. An expanded diagram of the mini optical composite is given in the inset of Fig. 2, where a scale bar is given. The schlieren system consists of a commercial Krypton light as a light source, a mini optical composite and four lenses, and has a total length of about 220 mm. The Kr-light passes

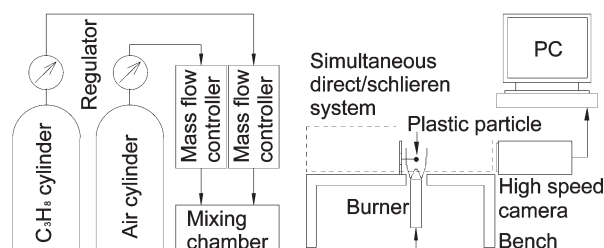


Fig.1 Schematic diagram of the experimental setup

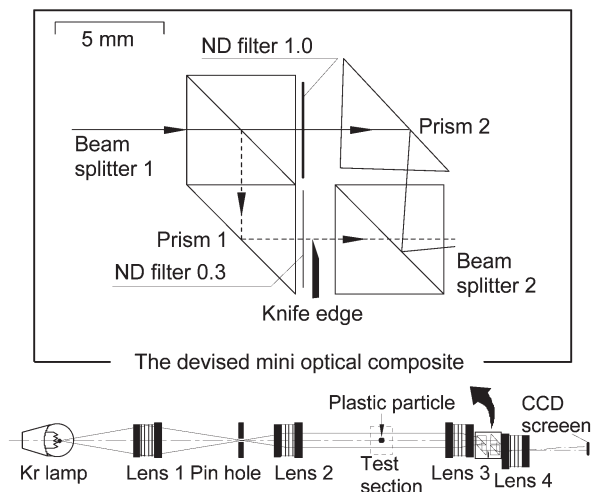


Fig.2 Arrangement of the mini schlieren system and an expanded mini optical composite

through lens 1 to focus on the pin hole having 0.5 mm diameter. After passing through lens 2, the Kr-light crosses the objective section as parallel light and enters into lens 3. To photograph direct silhouetted and schlieren images simultaneously, the parallel light through lens 3 including refracted light due to the density gradient in the objective section is brought into focus on the optical composite. As shown in the expanded inset of Fig. 2, a part of the focusing Kr-light is reflected at a right angle by cubic beam splitter 1, is reflected once again at a right angle by prism 1, and focuses on the knife edge after passing through a light shield filter (FUJIFILM ND-0.3, 50 % transmissivity). The parallel Kr-light goes straight through cubic beam splitter 2 and generates a uniform image on the CCD screen, whereas the refracted light included in the parallel light is intercepted by the knife edge to generate dark schlieren streaks on the CCD screen and constitutes a schlieren image around the micro PET particle. The other part of the focusing Kr-light goes through cubic beam splitter 1, passes through a light shield filter (FUJIFILM ND-1.0, 10 % transmissivity) to reduce the influence of the yellow flame emission, is reflected twice at a right angle by prism 2 and cubic beam splitter 2, and produces a direct transparent image on the CCD screen. It is important to emphasize that the proposed optical composite enables simultaneous observations of the direct silhouetted image and the schlieren image of the micro PET particle under a single rapid heating process.

The combined arrangement of the cylindrical mini-burner for abrupt heating and the mini-puff generator for sudden extinguishment at an arbitrary prescribed timing after the abrupt heating is schematically shown in Fig. 3. The mini-burner is made of a quartz glass tube having inner and outer diameters of 7 mm and 9 mm, from which a propane-air mixture having an assigned equivalence ratio of  $\phi = 0.84$  is issued vertically upward

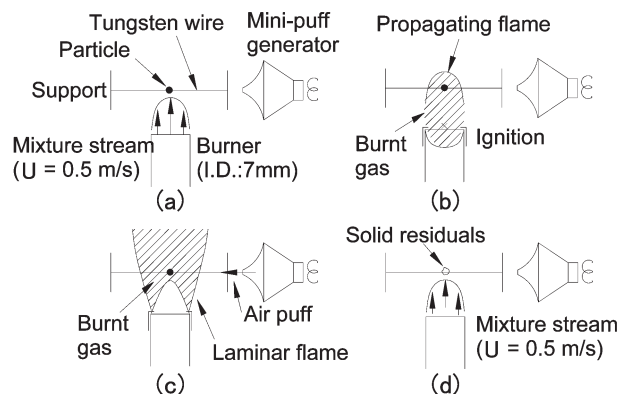


Fig.3 Combined arrangement of the mini-burner and the mini-puff generator, and a series of a single abrupt heating and extinguishment processes

at a mean velocity of  $U = 0.5$  m/s. A pair of spark needles having a gap of 5.8 mm and made of a tungsten wire of 200  $\mu\text{m}$  diameter is installed at the exit section of the mini-burner, and is discharged at an ignition energy of 21.9 mJ. The mini-puff generator is constructed by connecting a rectangular nozzle with a rectangular box with a side of 215 mm. The former nozzle having a length of 40 mm contracts the sectional area from 120 mm  $\times$  60 mm to 40 mm  $\times$  10 mm, and is placed horizontally so that the exit section is 50 mm apart from the plastic particle. A speaker having a cone diameter of 140 mm is equipped inside it. In a single abrupt heating and blow-off experiment, a combustion gas downstream of a spark-ignited propane-air lean premixed flame stabilized on the vertical circular mini-burner is used as an abrupt and oxidizing heat source, and the mini-puff generator is operated once at an arbitrary assigned timing after the abrupt heating using a delay time controller.

Four typical stages of a single abrupt heating and blow-off experiment can be seen schematically in Fig. 3(a)~(d). To improve the accuracy and reproducibility of image processing and to solve the problem how to support stationary a micro PET particle, spherically reformed particles having a diameter of about 200  $\mu\text{m}$  are used [2, 5, 9]. An original rugged PET particle is first attached to a fine tungsten wire of 5  $\mu\text{m}$  diameter and is heated to its melting point by radiation heat transfer from an incandescent Nichrome wire. Due to surface tension of the PET droplet, it rounds and condenses into a smooth spherical particle spitted by the tungsten wire. As shown in Fig. 3(a), a micro spherical PET particle reformed around a fine tungsten wire of 5  $\mu\text{m}$  is first placed on the axis of the propane-air lean mixture flow. Just after the spark ignition at the burner exit, a combustion wave is initiated and propagates in the downstream direction, as shown in Fig. 3(b), and a small conical laminar flame is stationary stabilized at the burner exit, as shown in Fig. 3(c). Abrupt heating starts at the instant when the high temperature

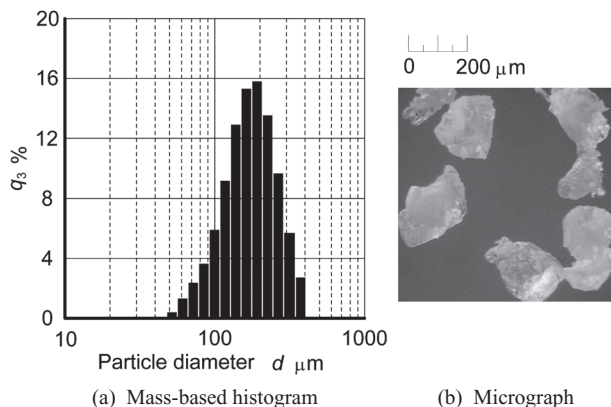


Fig.4 A mass-based histogram of original PET-powder and micrograph of PET particles sieved in the range of  $d > 180 \mu\text{m}$

Table 2 Physical and chemical properties of PET-resin [12-15]

Density	1380 [kg/m <sup>3</sup> ]
Melting point	523 ~ 548 [K]
Coefficient of linear expansion	$7.0 \times 10^{-5}$ [1/K]
Decomposition temperature	556 ~ 579, 673 ~ 923 [K]
Ignition temperature	759 [K]
Char content	17.0 [wt% at 973 K]
Main products of thermal decomposition	Benzene, Toluene, Styrene Terephthalic acid

oxidizing combustion gas passes through the supported PET particle. When the appearances of solid residuals after an arbitrary assigned heating time are observed and analyzed, the mini-puff generator is operated at the assigned timing after the abrupt heating to extinguish all flames around the PET particle, as shown in Fig. 3(d). A series of simultaneous direct and schlieren images after the abrupt heating is recorded using the high-speed CCD video camera operated at a framing speed of 500 fps.

Previous to the abrupt heating and blow-off experiment, a laminar lean premixed flame having an equivalence ratio of  $\phi = 0.84$  is first stabilized at the mini-burner. Temperature profile along the flame axis is then measured using a fine R-type thermocouple of 100  $\mu\text{m}$  diameter to determine the axial position of abrupt heating where temperature exhibits an assigned value of  $T_g = 1273 \text{ K}$  and a spherically reformed micro PET particle is stationary placed. In this paper the position of rapid heating is determined to be 35 mm downstream of the burner exit, where oxygen concentration is measured to be 12.3 %. Spherically reformed PET particles having an initial diameter of  $d_0 = 200 \pm 4 \mu\text{m}$  and a diameter deviation of  $\pm 2 \%$  are only used to improve the reproducibility of data acquisition.

A mass-based histogram of original PET-powder and an example of micrographs of PET-powder sieved in the range of  $d > 180 \mu\text{m}$  are presented in Fig. 4, where a scale bar is given

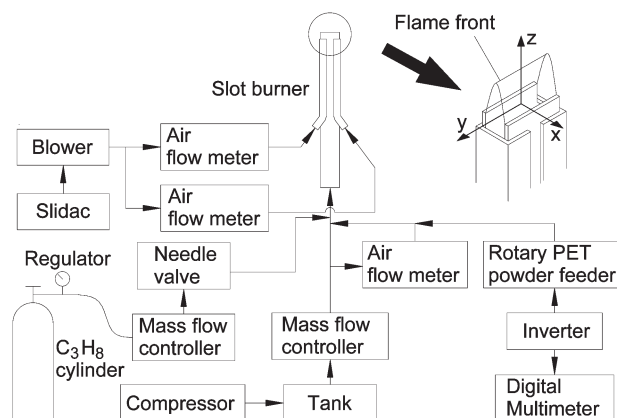


Fig.5 Schematic diagram of the experimental apparatus

on the top of the micrograph. It shows that the diameter of PET particle distributes widely in the range of  $d = 50 \sim 400 \mu\text{m}$  in spite of an assigned median diameter of  $d_m = 176.4 \mu\text{m}$ , and that PET particles exhibit ragged and irregular appearances. Typical physical and chemical properties of PET-resin are summarized in Table 2 [12-15]. It is found that PET-resin has a relatively low melting point and two different ranges of thermal decomposition temperature; 556 ~ 570 and 673 ~ 923 K. Also found is that the main products of thermal decomposition are all aromatic compounds, and that they are well-known to be typical precursors for soot formation.

### 3.2. High-Speed Magnifying and Tracking System

The schematic diagram of the experimental system for the high-speed magnifying and tracking observation is presented in Fig. 5. The system consists of a propane-air mixture supply line, a PET powder supply line, a two-dimensional slot burner, and an air supply line for preventing premixed flames from anchoring on the short side rims of the burner. The arrangement of the optical tracking system is shown in Fig. 6, where the  $x$ - $y$ - $z$  rectangular coordinate system of the two-dimensional burner and the relative positioning of two rotating mirror axes are indicated. The optical tracking system is composed of a green laser diode (Kyoritsu Denshi Sangyo, L532-3G-3-P, a maximum output of 5 mW), two rotating Mirror 1 and 2, a plane surface Mirror 3, and a high-speed CCD video camera (Photron, FASTCAM-PCI, 1000 fps). Mirror 1 is constructed using a pair of two plane surface mirrors of 5 mm thickness installed on two opposite sides of a rectangular rod having a side of 35 mm, whereas Mirror 2 is made of two pairs of the same four plane surface mirrors of 5 mm thickness fixed on four sides of a rectangular rod having the same side of 35 mm. All plane surface mirrors including Mirror 3 have the same dimensions of 35 mm width and 126 mm length.

A green laser diode is used as a light source, since PET powder burns as diffusion flames with intense yellow emission. The

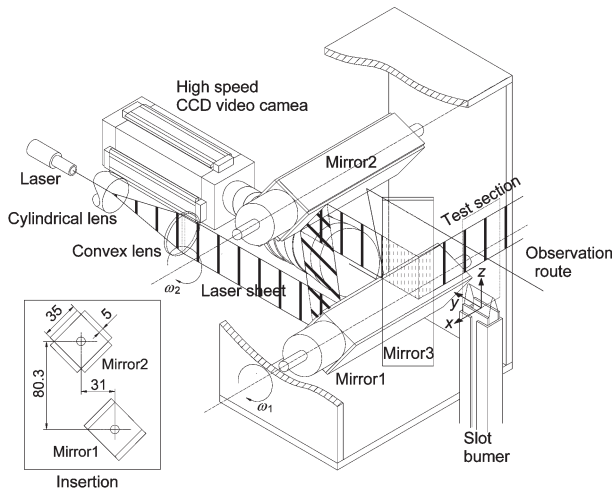


Fig.6 Construction and arrangement of the devised optical tracking system combined with a high-speed video camera

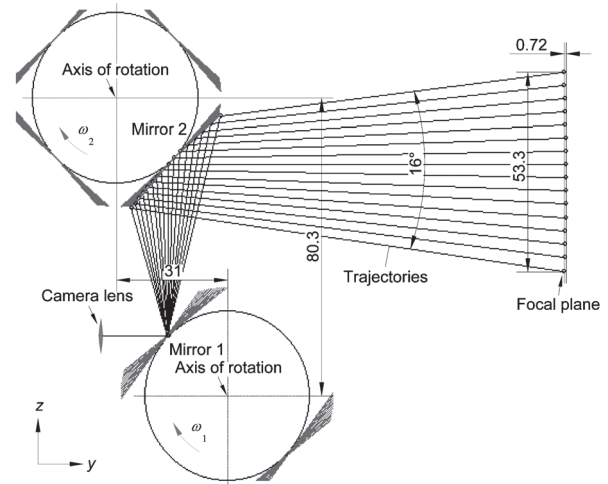


Fig.7 A series of optical trajectories simulated under the optimum mirror arrangement and the optimum ratio of angular velocity

green laser beam passes successively through a cylindrical lens and a convex lens to form a laser sheet having a thickness of 0.6 mm and a height of 30 mm, is reflected twice at Mirror 1 and Mirror 2, and is introduced into the flame zone in the  $x-z$  plane, after reflecting again at a right angle at Mirror 3. The high-speed CCD video camera takes a series of tracking images of PET particles. The high-speed camera is stationary fixed and operated at a framing speed of 1000 fps, while the rotating speed of Mirror 1 is set in the range of 80 ~ 100 rpm.

To obtain the optimum arrangement for Mirror 1 and 2 and the optimum ratio of angular velocities by fixing the high-speed CCD video camera stationary, a series of simulations is carried out by varying the relative distances between the axes of Mirror 1 and 2 and the ratio of angular velocities, the former being mainly prescribed by the focal length of the optical system used. The simulation results indicate that not only the longest particle passage in the axial direction, but also the minimum deviation in the depth is obtained, when the axes of Mirror 1 and 2 are set 31 mm apart along the  $y$ -axis and 80.3 mm apart along the  $z$ -axis and the ratio of the angular velocity of Mirror 1 to that of Mirror 2 is set equal to  $\omega_2/\omega_1 = 0.5$ . A set of optical tracking trajectories obtained under the optimum condition is given in Fig. 7. It shows that a tracking angle of  $16^\circ$ , an axial tracking distance of  $\Delta z = 53.3$  mm and a deviation in the depth of  $\Delta y = 0.72$  mm are realized. An extremely small deviation rate of  $\Delta y/\Delta z = 0.013$  proves excellent linearity of the tracking trajectory of the proposed rotating mirror system.

As shown in Figs. 6 and 7, two sets of plane surface mirrors are used to improve the imaging efficiency by composing Mirror 1 by two diagonal plane surface mirrors and Mirror 2 by four plane surface mirrors on four sides, and the angular velocity of Mirror 1 is set twice that of Mirror 2. When the proposed system

is operated at the prescribed setting conditions, the imaging efficiency becomes fourfold as high as it is operated using each one of Mirror 1 and Mirror 2 at the same angular velocity. In this paper, however, each one plane mirror of Mirror 1 and 2 is used and operated at the prescribed rotation velocity as the first step of the optical tracking observation.

In this experiment the two-dimensional cold flow field in the  $x-z$  plane without combustion is first measured using a constant temperature type hot-wire anemometer equipped with an I-type probe (Hayakawa Sokken, Model HC-30 and HC-25-5I). The two-dimensional temperature field across the flame is then measured in the  $x-z$  plane using a head-on-welded R-type fine thermocouple of 100  $\mu\text{m}$  diameter. No compensation is made on the results measured. The velocity vector field across the two-dimensional premixed flame is then measured using a PIV/PTV system, which is composed of a Double Pulsed Nd:YAG Laser (Continuum, CLP10PIV) having a maximum output of 220 mJ/pulse, a pulse width of 5 ns and a wave length of 532 nm and a high-speed CCD camera (Ikegami, SKC-133). Plaster powder for dental use having an average diameter of 20  $\mu\text{m}$  is used as tracer particles for PIV measurements, whereas PET-powder is used for PTV measurements. In the latter case PET-powder having a median diameter of  $d_m = 176.4 \mu\text{m}$  is sieved in the range of  $d > 180 \mu\text{m}$  to make observation of their ignition and burning processes easy and clear. Appearances of sieved PET particles can be seen in Fig. 4(b). Commercial LPG having a propane purity of 96.4 % is used for both the cylindrical burner and the two-dimensional slot burner.

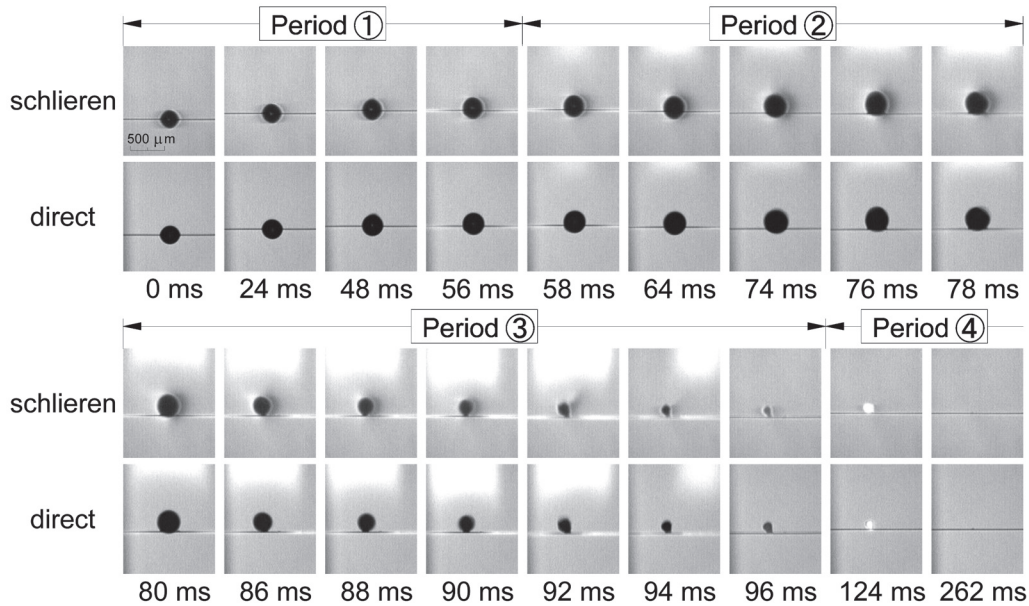


Fig.8 A series of high-speed direct and schlieren images of a micro spherical PET particle under the abrupt heating, where  $d_0 = 200 \mu\text{m}$ ,  $\phi = 0.84$ ,  $T_g = 1273 \text{ K}$ , where the shutter speed and exposure time are set to 500 fps and 1 ms.

## 4. Experimental Results and Discussion

### 4.1. High-Speed Direct and Schlieren Images of a PET Particle under Abrupt Heating

#### 4.1.1. Appearances of PET particle during abrupt heating

High-speed simultaneous direct and schlieren images of a spherical PET particle having an initial diameter of  $d_0 = 200 \mu\text{m}$  are shown in Fig. 8. The upper and lower photos give the schlieren and direct silhouetted images, respectively, and the number given at the bottom of each set of images indicates the time after the abrupt heating. The equivalence ratio of propane-air mixture and the heating temperature are assigned to  $\phi = 0.84$  and  $T_g = 1273 \text{ K}$ , respectively. The framing speed and the exposure time of the high-speed CCD camera are set to 500 fps and 1 ms. A scale bar is given in the first schlieren image in Fig. 8 for easy evaluation of the particle size.

Variation of the particle diameter  $d$  and surface area  $d^2$  with the time  $t$  is examined by processing a series of high-speed direct and schlieren images given in Fig. 8. The results are summarized in Fig. 9, where the ordinates give the particle diameter  $d$  and the particle surface area  $d^2$ , and the abscissa indicates the time  $t$  after the abrupt heating. For easy understanding of the particle behavior after the abrupt heating, some typical schlieren images are inserted in Fig. 9. The use of spherically reformed particles within a diameter deviation of  $\pm 2 \%$  enables high reproducibility in the determination of characteristic timings within a deviation of a few milliseconds.

According to Fig. 8, first, almost no change is found in the

initial period of  $t \leq 54 \text{ ms}$ , except for slight volumetric expansion due to temperature rise of the PET particle. At  $t \approx 56 \text{ ms}$ , a dark thin schlieren streak can be observed around the particle. Since a small diffusion flame is just observed in the wake region of the particle, it is found that thermal decomposition and gasification start and are followed by combustion at this timing. In the time duration of  $t = 58 \sim 78 \text{ ms}$ , the PET droplet stands against the gas flow and barely clings to the tungsten wire while it dances around on the top of the wire. During the same time duration, the diameter of PET droplet exhibits a remarkable increase up

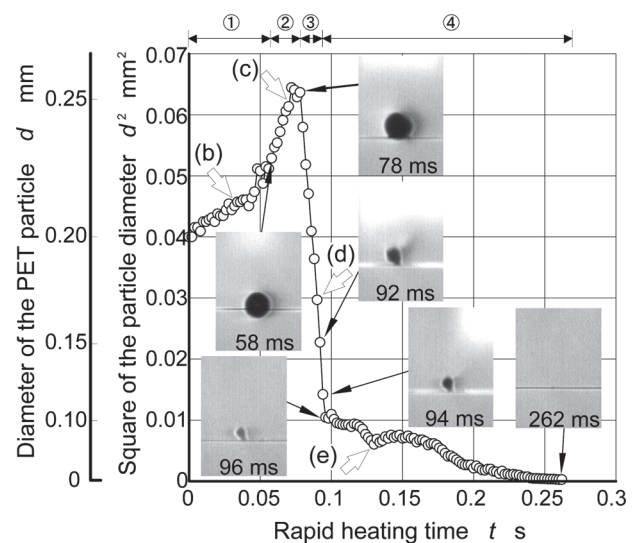


Fig.9 Temporal variation of the diameter and surface area of a PET-resin particle, where  $\phi = 0.84$  and  $T_g = 1273 \text{ K}$

to about 1.25 times with the thin dark schlieren streak around it almost unchanged. Since the volumetric expansion rate of 1.95 ( $= 1.25^3$ ) is considered to be too large to be realized only by thermal expansion, such a great volumetric expansion rate of 1.95 needs other factors. These temporal variations can be seen in Fig. 9 as a two-step increase in the particle surface area.

After reaching its maximum at  $t \approx 78$  ms, the surface area of PET droplet becomes quickly smaller and smaller as thermal decomposition, gasification and combustion proceed, and a wake type yellow diffusion flame blows out at  $t \approx 96$  ms in concert with the termination of gasification. In this time duration of  $t = 78 \sim 96$  ms, the surface area of PET droplet decreases almost linearly with the time after the abrupt heating. The quick reduction of droplet surface area is followed by a slow reduction period due to surface combustion of solid residuals and results in a discontinuous change in the gradient, as can be seen in Fig. 9. Since surface combustion of solid char requires an extremely long time, the total life time of PET particle becomes longer.

Based on these detailed observation and consideration of Figs. 8 and 9, the entire heating process of a micro PET particle is found to be qualitatively divided into four periods. The first is the moderate volumetric expansion period due to temperature rise, the second is the prominent volumetric expansion period due to moderate thermal decomposition and gasification, the third is the steep reduction period of the particle surface area due to violent thermal decomposition and gasification followed by multiple micro explosions and combustion, and the fourth period is composed of the slow reduction of surface area due to surface combustion of residual char. In Figs. 8 and 9, these four divisions are already given for easy understanding. In the following of this paper, main attention will be paid to the key factors which enable the remarkable volumetric expansion in the second period and the quick reduction of the surface area, and the dependency of appearances and internal structure of solid residuals on the heating time after the abrupt heating will be examined.

#### 4.1.2. Internal and external structure of PET resin embers

The heating process of a spherical micro PET particle is ceased separately and several times at four assigned instants, which are indicated by the white arrows in Fig. 9. Typical micrographs of PET embers are shown in Fig. 10. It should be noted here that these micrographs are taken separately under room temperature after ceasing the heating process at four assigned timings and that, accordingly, the volumetric expansion of micro bubbles due to temperature rise does not appear in Fig. 10.

Figure 10(a) gives an example of micrographs of an initial spherically reformed PET particle and shows smooth and transparent appearances. This result indicates that the original properties of PET resin do not change by radiation heating in the

reforming process. The embers obtained by ceasing the heating process at the assigned timing of  $\tau = 30$  ms at the middle of the first period, as shown in Fig. 10(b), has almost the same smooth and transparent appearances as those of the initial particle, except that several micro bubbles are apparent in the particle. When the heating process is continued and is ceased at the assigned timing of  $\tau = 70$  ms in the second period of remarkable volumetric expansion, however, a lot of micro bubbles can be observed in the PET embers, as given in Fig. 10(c). Based on these results, the following qualitative consideration can be made. The main products of thermal decomposition of PET-resin are Benzene, Toluene and Styrene. They have lower saturation points ranging 353 ~ 418 K [16] than the thermal decomposition temperature of PET-resin as given in Table 2 [12-15]. As a result, multiple and internal thermal decomposition is instantaneously followed by multiple gasification within the liquid PET particle, leads to multiple internal micro bubbling, and finally results in an apparent large volumetric expansion rate up to about 1.95. It is also observed that the color of PET-resin embers gradually becomes dark brown as the thermal decomposition proceeds.

Figure 10(d) shows clearly that the PET embers contain multiple finer spherical bubbles having diameters of  $d = 13 \sim 24 \mu\text{m}$  and exhibit an irregular and rugged shape, when the heating process is ceased at the middle point of the third quick reduction period,  $\tau = 90$  ms. Taking account of the unstable and irregular behavior of PET droplets on the tungsten wire in the third prompt reduction period, which can be observed in Fig. 8, these results prove that, due to violent thermal decomposition and instantaneous gasification, the multiple internal micro bubbling becomes more and more remarkable in the third period and is followed instantaneously by multiple and irregular micro explosions and jets and micro diffusion flames around the PET droplet. It is considered here that the thermal decomposition and instantaneous gasification first causes the multiple internal micro bubbling within the PET droplet, the multiple internal micro bubbling is then followed by intense multiple micro explosions and jets, and the combined effect of these multiphase chemical and physical processes constitutes the key factor to the violent gasification of PET droplet and results in the steep reduction of the droplet surface area. It is interesting to note here that even a series of heating processes of such fine PET particles having diameters of about  $200 \mu\text{m}$  is controlled by multiple internal micro bubbling having finer scales of about a tenth of the original particle diameter.

When the heating process is continued finally to the fourth period of slow surface combustion, the irregular appearances of PET embers remain almost unchanged. The micrograph given in Fig. 10(e) indicates that the PET ember is colored almost black and consists of micro spherical char bubbles having finer diameters than those in the third period.

Table 3 Comparison of burning rate constants [ $\text{mm}^2/\text{s}$ ] [17]

PET	Diesel light oil	Benzene	Iso-octane
$d_0 = 200 \mu\text{m}$ $T_g = 1273 \text{ K}$ $12.3 \% \text{ O}_2$	$d_0 = 1 \text{ mm}, T_g = 1268 \text{ K}, \text{ Air (21 \% O}_2)$		
3.00	2.15	1.40	1.35

#### 4.1.3. Apparent burning constant of micro PET particles

As described in the preceding paragraphs, the temporal variations of the surface area of PET droplets exhibit fine linear reduction in the third heating period. Although evaporation does not occur in plastic-resin, the temporal variation of the droplet surface area during the third heating period is examined by simply replacing “evaporation” with “thermal decomposition and gasification”, and the  $d^2$ -law for quasi-steady combustion of liquid fuel droplets is adopted here. The method of least squares applied to the third period of the abrupt heating process shown in Fig. 9 gives a gradient of linear reduction of  $C_b = 3.00 \text{ mm}^2/\text{s}$ , being an apparent burning rate constant of the micro PET droplet. This burning rate constant is now compared with those of well-known typical volatile liquid fuels. Under the conditions of an initial droplet diameter of 1 mm and a surrounding air temperature of 1268 K, the burning rate constant of diesel light oil, benzene and iso-octane takes a value of  $C_b = 2.15 \text{ mm}^2/\text{s}$ ,  $1.40 \text{ mm}^2/\text{s}$  and  $1.35 \text{ mm}^2/\text{s}$ , respectively [17]. These values of the burning constant are summarized in Table 3.

The burning rate constant of a micro PET droplet,  $C_b = 3.00 \text{ mm}^2/\text{s}$ , is found to be greater than those of the typical volatile liquid fuels under nearly the same temperature condition. For example, the value of  $C_b = 3.00 \text{ mm}^2/\text{s}$  is greater than that of diesel light oil by about 40 % and that of iso-octane by about 2.2 times. Taking into account of the fact that PET-resin does not contain volatile materials and has a relatively high decomposition temperature range of 556 ~ 923 K, these results suggest the following qualitative scheme for yielding such a high burning rate constant. The larger surface area to volume ratio particular to a micro particle due to its smaller initial diameter highly promotes heat transfer around the particle and causes violent internal bubbling due to intense thermal decomposition of PET-resin and instantaneous gasification of decomposed products. The multiple internal bubbling is followed by multiple irregular micro explosions and irregular micro jets. The multiple micro explosions and jets, in turn, enhance heat and mass transfer to and from the particle by disturbing and breaking the boundary layer around the micro droplet, resulting finally in an extremely high burning rate constant which is higher than those of highly volatile liquid fuel droplets. The highly promotive effects of multiple internal bubbling and multiple micro explosions, accordingly, overcome a negative factor caused by the use of

combustion gas having a low oxygen concentration, instead of high temperature normal air. It is therefore clarified that micro plastic resin particles having greater surface to volume ratios and subjected suddenly to high temperature oxidizing circumstances exhibit high volumetric expansion rates and high burning rate constants due to the combined effect of multiple internal micro bubbling, multiple micro explosions and multiple micro jets.

## 4.2. High-Speed Magnifying and Tracking Images of PET Particles Passing through a Premixed Flame Sheet

### 4.2.1. Flow and temperature properties of a slot burner

The proposed two-dimensional premixed burner having a width of 9.6 mm and a depth of 22.6 mm enables formation of a laminar flame with fine two-dimensionality, since a pair of plane air jets is issued along the both short sides at a mean velocity of 3.6 m/s and prevents premixed laminar flames from anchoring to the short side rims. In Fig. 11, an example of direct photographs of the two-dimensional laminar premixed flame is shown, where Fig. 11(a) gives its side view and (b) presents its front view. The average propane-air mixture velocity and its relative turbulence intensity are  $U = 1.5 \text{ m/s}$  and  $u'/U = 2.5 \%$ , respectively, and the equivalence ratio of propane-air mixture is set to  $\phi = 0.9$ .

Figure 11(a) gives clearly a pair of roof-shaped flame sheets with an entirely transparent front-flame zone in their upstream region, whereas Fig. 11(b) exhibits uniform appearances of flame surface with extremely uniform blue emission. The distinct two-dimensionality can prepare a uniform high temperature oxidizing region symmetrically behind the planar flame sheets on both long sides of the burner and, therefore, can realize not only uniform and abrupt heating of PET particles, but also acquisition of clear images of PET particles passing through either of the flame sheets.

By taking best use of the fine two-dimensionality of the proposed premixed slot burner, the laminar burning velocity is briefly estimated. The angle method results in the burning velocities of  $S_u = 0.33 \text{ m/s}$ ,  $0.40 \text{ m/s}$  and  $0.38 \text{ m/s}$  at the upstream point ( $x = 3 \text{ mm}$ ), at the middle stream point ( $x = 2 \text{ mm}$ ) and at the downstream point ( $x = 1 \text{ mm}$ ) along the flame sheet, respectively. The simply averaged burning velocity of  $S_u = 0.37 \text{ m/s}$  for the equivalence ratio of  $\phi = 0.9$  exhibits excellent agreement with those obtained experimentally by Harris et al.;  $S_u = 37.3 \text{ cm/s}$  ( $\phi = 0.92$ ) [18], and Yamaoka and Tsuji;  $S_u = 36.6 \text{ cm/s}$  [19], verifying fine two-dimensionality of the proposed premixed burner.

Two-dimensional velocity vector and temperature fields in the  $x$ - $z$  plane of the flame are shown in Fig. 12, where the temperature field is presented as iso-thermals in K and is reversed symmetrically with respect to the  $z$ -axis. The flame zone is presented by an oblique dense zone consisting of multiple iso-

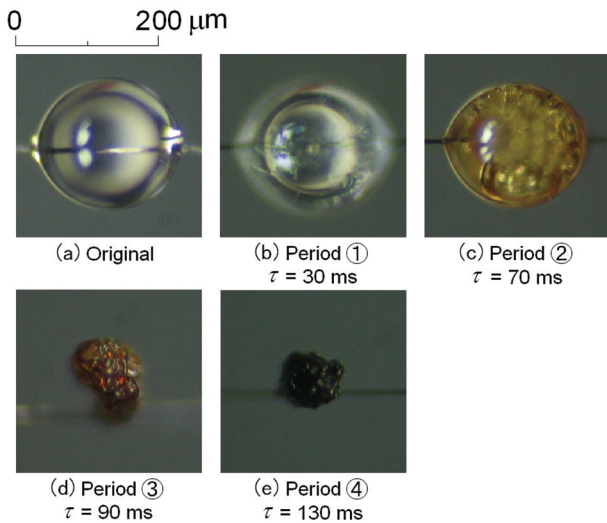


Fig.10 Examples of micrographs of PET-embers obtained at four assigned blow-out timings

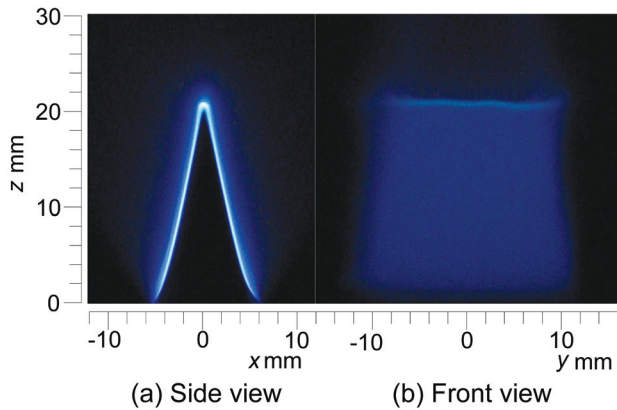


Fig.11 Side and front views of two-dimensional premixed propane-air flame, where  $\phi = 0.9$  and  $U = 1.5$  m/s

thermals in the temperature field, whereas it is schematically indicated by an oblique fine solid line in the right vector diagram.

According to the temperature field, first, it is found that the flame zone has a thin thickness of about 1 mm and constitutes a clear boundary between a low temperature mixture zone and a high temperature combustion gas zone, resulting in an extremely steep temperature gradient. The temperature in the latter hot gas zone is maintained almost constant and uniform in the range of  $T_f = 1873 \sim 1973$  K. These features are very favorable for making possible abrupt heating with negligibly small effect of preheating, when PET particles enter into the flame zone. The vector diagram indicates clearly that, on the other hand, the tracer particles are accelerated and refracted outward with their passage through the flame zone. Almost no error vector can be observed in the diagram, indicating high accuracy of PIV-measurements.

Based on the results obtained above, brief consideration is made on the flow fields across the flame sheet. The angle of velocity

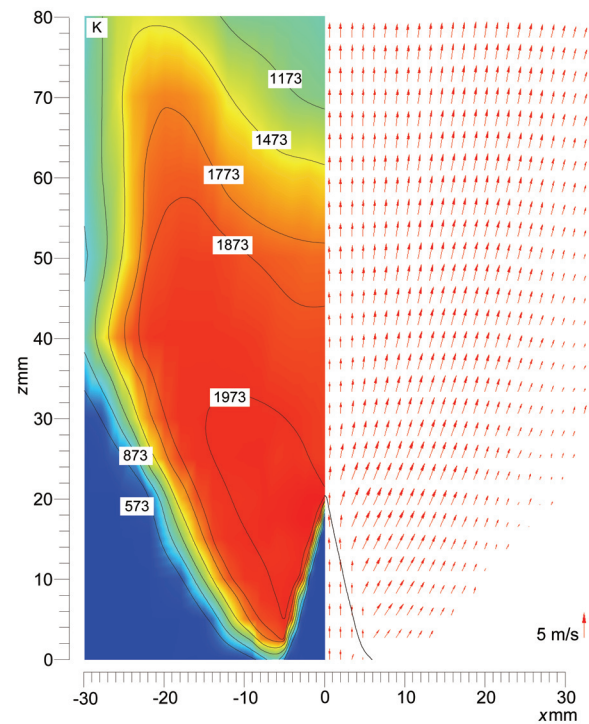


Fig.12 Temperature and velocity vector fields in the  $x$ - $z$  plane of the proposed two-dimensional premixed flame

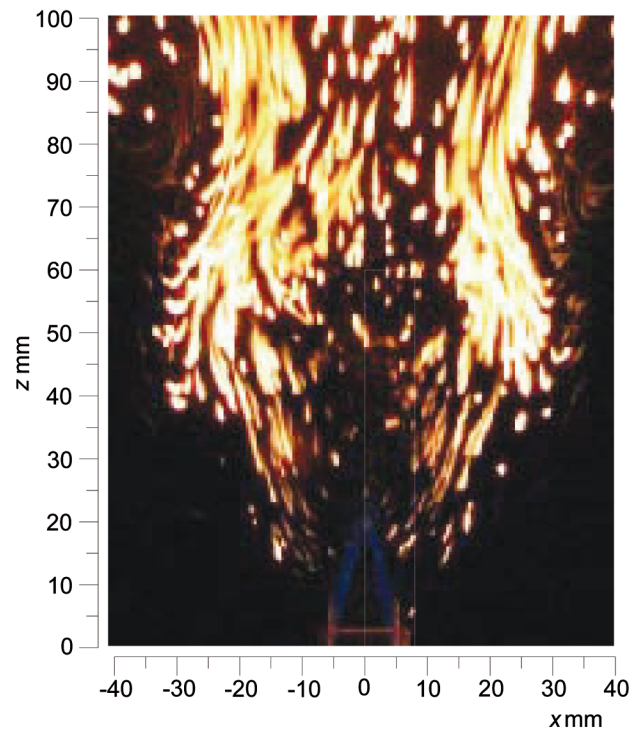


Fig.13 An example of instantaneous direct photographs of PET-powder diffusion flames, where  $d_m = 176.4 \mu\text{m}$  and  $m_{\text{PET}} = 4.8$  g/min

vectors just behind the flame sheet varies roughly in the range of  $45^\circ \sim 55^\circ$  with respect to the normal to the flame sheet, whereas their magnitude varies correspondingly in the range of  $3.0 \sim 3.6$  m/s. These values mean that the combustion gas leaves the

flame zone at a nearly constant velocity of 2.1 m/s normal to the flame sheet. The latter velocity agrees relatively well with that estimated by using the mean burning velocity of  $S_u = 0.37$  m/s and the temperatures just before and behind the flame sheet, 300 K and 1973 K respectively, within a deviation of about 15 %.

#### 4.2.2. Magnifying and tracking images of PET particles flying through a premixed flame sheet

When PET powder having a median diameter of  $d_m = 176.4$   $\mu\text{m}$  is supplied into the proposed propane-air lean premixed flame at a mass flow rate of  $m_{\text{PET}} = 3.4$  g/min, a yellow diffusion flame is established downstream of the slot burner. An example of instantaneous direct photographs of brilliant PET powder diffusion flames taken obliquely below along the  $y$ - $z$  plane is shown in Fig. 13, where the observation region for high-speed magnifying tracking is indicated by a white rectangular for reference. According to Fig. 13, a pair of two blue flame sheets can be observed just downstream of the burner, although it appears somewhat indistinct and thick roof-shaped due to the oblique field of vision. It is found that PET particles enter into the flame zone, are heated up to their decomposition temperature, ignite spontaneously, burn as they pass through the high temperature post-flame zone just downstream of the planar premixed flame, and finally exhibit multiple incandescent stripes of yellow diffusion flames with long tails of several to more than ten millimeters.

In this paper main attention is paid to magnifying and tracking observation of a series of multiphased physical and chemical processes of PET particles after entering into and passing through the flame zone. Based on detailed analysis of the results, various types of yellow diffusion flames can be distinguished, such as wake-type flames and envelope-type flames with and without a long tail, depending on the particle velocity and the magnitude and direction of the relative velocity between the particle and the ambient gas flow. In this section, two typical examples of micro diffusion flames are presented and analyzed; one is a wake flame having a long tail behind it in the downstream direction, the other is a wake flame with a long tail in the upstream and exhibiting special appearances in its final burning stage. In the following these two types of micro diffusion flames are examined in detail.

A series of high-speed and magnifying tracking images of PET particles flying through the high temperature post-flame zone downstream of the proposed plane premixed flame is shown in Fig. 14, where Fig. 14(a) indicates the tracking domain by a series of white squares and the particle position by a series of white small circles, and Fig. 14(b) gives 18 frames of high-speed images along with the axial distance  $z$  from the burner exit on their bottoms. For easy estimation of the particle and flame sizes, a scale bar is given on the top of Fig. 14(b). In this case, as given by the  $z$ -value at the bottom of each figure of ①-⑱, the position

of PET particle changes from  $z = 22.5$  mm to 55.0 mm during the magnifying and tracking observation.

As pointed out by the white arrow in Fig. 14(b)-①, a PET particle comes insight into the laser sheet at the upper-left part of the frame, melts and decomposes thermally during its relative movement in the downstream direction, and becomes clear and clear, as can be seen in Fig. 14(b)-②~⑦. At the position of  $z = 35.9$  mm, a weak yellow flame is generated behind the PET droplet, as indicated by the arrow in Fig. 14(b)-⑧, and grows with relative movement in the downstream direction to form a small wake flame having a length of about 0.3 mm at  $z = 37.8 \sim 39.8$  mm, as can be seen in Figs. 14(b)-⑨ and ⑩. According to the flame shape around the particle, the relative velocity between the particle and the hot combustion gas flow is considered to be very small in the upstream region of  $z = 23 \sim 40$  mm. In further downstream movement, however, the flame shape changes to a long-tailed wake flame having a length of about 3 mm at  $z = 49.1$  mm, as indicated in Fig. 14(b)-⑮. The downstream growth of wake type flame means that the hot combustion gas flows faster than the PET particle in the downstream region of  $z > 40$  mm. Due to the limited view of the high-speed CCD camera in the  $x$ -direction, further development of the long-tailed diffusion flame can not be observed. By taking account of the observation results concerning Fig. 13, however, it may be expected that the wake flame grows further to become an extremely long wake flame up to several to more than ten millimeters.

According to the detailed image processing of flying PET particles presented, for example, in Fig. 14(b)-④~⑨, a series of the multiphased physical processes that an original rugged PET particle is heated up to its melting point, melts and is reformed into a spherical one having a diameter of about 150  $\mu\text{m}$  due to surface tension of liquid droplets can be relatively clearly observed. These particle behaviors under abrupt heating agree well with those observed in the preceding investigation with respect to the variations of the shape and diameter of flying PET particles in the industrial burner [5].

A series of magnified tracking images of those two long-tailed wake flames behind micro PET particles which changes their appearances into a long and thin cluster of multiple micro brilliant spots in the final period of burning processes is shown in Fig. 15. A scale bar is also given on the top of Fig. 15(b). Two PET particles are simultaneously tracked and, as indicated by the  $z$ -value at the bottom of each figure of Fig. 15(b)-①~⑮, the positions of PET particles vary in the range of  $z = 32.0 \sim 57.4$  mm. It is found that, different from those in Fig. 14(b), all long-tailed flames observed in these figures grow to the upstream direction, and that the two PET particles fly faster than the ambient combustion gas, although it appears as if they were floating in the quiescent hot combustion gas. These results indicate clearly prominent influences of the relative velocity on

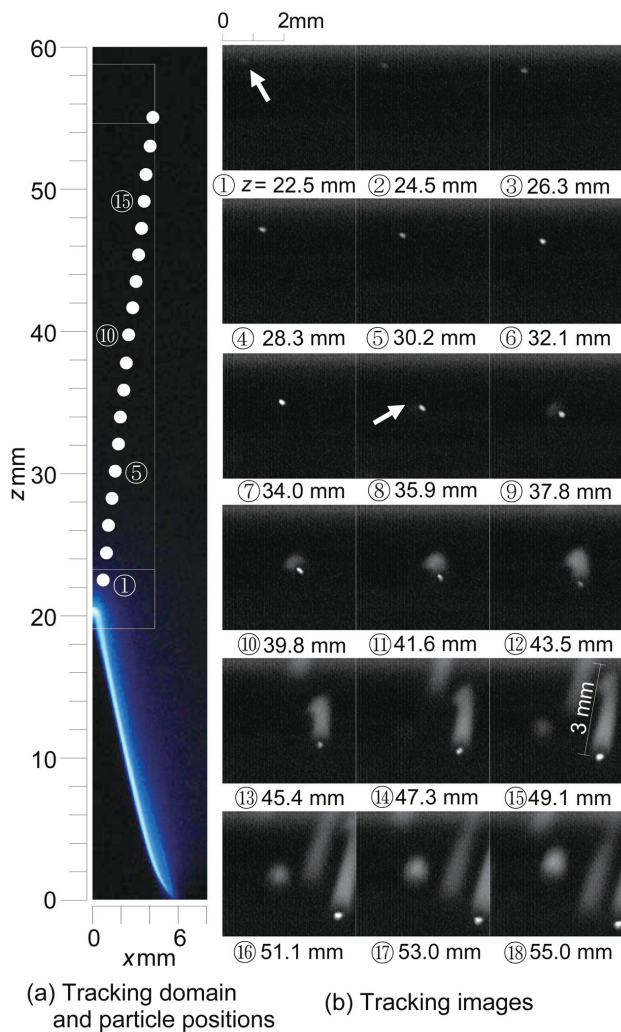


Fig.14 A series of high-speed magnifying and tracking images of PET particles flying in the hot post-flame region: appearances of long-tailed wake flames

the flame patterns around the PET particles.

It is extremely interesting that, as indicated by two pairs of arrows in Fig. 15(b), a slender envelop flame changes to a long and thin cluster consisting of multiple micro brilliant spots within a short passage of  $z = 45.9 \sim 49.3$  mm and  $z = 51.9 \sim 55.5$  mm respectively, being only a few millimeters and milliseconds. The average diameter of brilliant spots is estimated to be from more than ten to several tens micrometers. The latter type of flame patterns is called here as a long-tailed speckled flame for simplicity of explanation. At this point, however, only qualitative consideration is apparent with respect to the transformation mechanism of the slender envelope flame to the long-tailed speckled one. By taking account of the chemical properties that, as already shown in Table 2, the main products of thermal decomposition of PET resin are benzene, toluene and styrene and contain benzene nucleus [12-15], it is considered that soot particles generated in the highly rich diffusion flame zone would

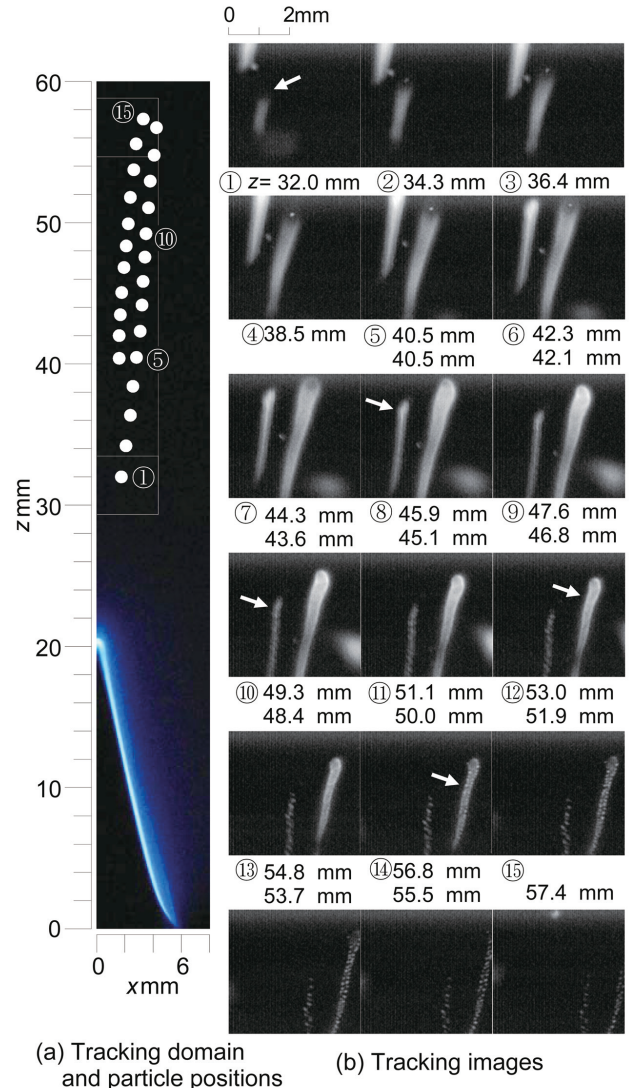


Fig.15 A series of high-speed magnifying and tracking images of PET particles flying through hot post-flame region: appearances of long-tailed envelop and speckled flames

coagulate to multiple speckled spots as they are generated and burn. It may also be considered that, due to the shearing force caused by the velocity difference between the liquid PET particle and the ambient hot gas flow, the micro PET-droplet is further dispersed into finer PET-fog along the long-tailed trajectory as it burns. The detailed mechanism, however, is remained unsolved here and constitutes one of the most important future subjects to be investigated in detail.

Based on these results, it is emphasized that, in spite of such micro PET particles as having small diameters of a few hundreds micrometers, the multiphase processes of melting and thermal decomposition of PET particles, the ignition and combustion processes of gasified PET resin, and the behavior of diffusion flames around or behind PET particles can be precisely observed and analyzed by using the proposed high-speed and magnifying

tracking system combined with the proposed fine two-dimensional slot burner.

## 5. Conclusions

In this paper, the abrupt heating process of a spherical micro PET particle is observed by combining the high-speed microscopic direct and schlieren system with the premixed mini-burner for abrupt heating. Dependencies of internal and external appearances of PET residuals on the heating time after the abrupt heating are also optically examined by using further the single mini-puff generator. A series of multiphase processes of micro PET particles under abrupt heating is also made by combining the proposed high-speed and magnifying particle tracking system with the proposed laminar premixed slot burner. The results are summarized as follows.

(1) The entire heating process of a micro PET particle is qualitatively divided into four distinct periods; the moderate volumetric expansion, the remarkable volumetric expansion, the steep reduction of the PET surface area, and the slow surface combustion of residuals.

(2) In the first solid heating and melting period, the spherical micro PET particle exhibits moderate volumetric expansion due to temperature rise. A few micro bubbles are generated due to thermal decomposition and gasification. Once thermal decomposition occurs in the droplet, however, instantaneous gasification of decomposed products leads to multiple internal micro bubbling and, therefore, to an apparent great volumetric increase in the second period. The embers obtained in this period contain many micro bubbles within them and prove these qualitative considerations.

(3) Violent internal micro bubbling due to multiple thermal decomposition and quick gasification promotes multiple micro explosions and micro jets in the third period. The multiple micro explosions and jets enhance heat and mass transfer and, in turn, augment thermal decomposition. It is concluded that the cyclic effects of intense thermal decomposition and rapid gasification, multiple internal micro bubbling, multiple micro explosions and multiple micro jets realize high burning rate constants. The embers obtained in the third period consist of finer multiple bubbles and exhibit irregular appearances.

(4) The proposed propane-air premixed burner exhibits extremely fine two-dimensionality and provides uniform and nearly constant high temperature post-flame region downstream of the laminar flame. This makes possible abrupt and continuous heating of PET particles when they enter into and pass through the flame zone.

(5) The proposed high-speed and magnifying tracking system composed of a pair of synchronized rotating plane mirrors and a high-speed video camera makes possible the long range particle-

tracking of PET particles up to about 50 mm with an extremely small deviation of 0.7 mm in the depth, even using a stationary fixed high-speed camera.

(6) Various magnifying tracking images of PET particles having diameters of about 200  $\mu\text{m}$  clarify many interesting behaviors. Depending on the relative velocity between the particle and the ambient gas flow, the patterns of yellow diffusion flames are classified into a wake type and an envelop type, their length varies in the range from several hundreds micrometers to more than ten millimeters, and a long-tailed envelop flame changes into a long-tailed speckled flame, the latter being composed of multiple micro brilliant points having diameters of several tens micrometers.

## Acknowledgments

This investigation is financially supported in part by *Tanikawa Foundation*, for which the authors express their sincere thanks. The authors also greatly acknowledge Mr. Kosuke Nishino, Mr. Yuki Kato, Ms. Mino Tochigi, Mr. Takanori Tomatsu, Mr. Atsunori Yamamoto, Mr. Tatsuhiko Nakama, and Mr. Takashi Fukuroda for their strenuous and faithful contribution to this investigation.

## References

1. Yamakita, R., Miura, K., Ishino, Y. and Ohiwa, N., An Investigation on Thermal Recycling of Recycled Plastic Resin (Combustion Characteristics of Polyethylene Terephthalate Resin Powder in a High Temperature Oxidizing Atmosphere), *JSME International Journal*, **48**-1B, 83-91 (2005).
2. Yamakita, R., Ishino, Y. and Ohiwa, N., Appearances of Multiple Micro Explosions, Micro Jets and Micro Diffusion Flames around an Abruptly Heated Micro Plastic Resin Particle, *Proceedings of the 5th Asia-Pacific Conference on Combustion*, 209-212 (2005).
3. Yamakita, R., Sato, T., Ishino, Y. and Ohiwa, N., An Investigation on Thermal Recycling of Recycled Plastic Resin (PIV/PTV Measurements of Flow Characteristics and Appearances of Flying PET-Particles in the Improved Industrial Burner), *Transactions of JSME*, (in Japanese), **72**-713B, 187-193 (2006).
4. Yamakita, R., Ishino, Y. and Ohiwa, N., An Investigation on Thermal Recycling of Recycled Plastic Resin (Spherically Symmetric Analysis of Abrupt Heating Processes of a Micro Plastic-Resin Particle), *Heat Transfer-Asian Research*, **35**-4, 279-293 (2006), Wiley Periodicals.
5. Yamakita, R., Ishino, Y. and Ohiwa, N., Optical Analyses of Burning Processes of Recycled Plastic Resin Powder, *International Journal of Transport Phenomena*, **8**, 223-237

- (2006), Old City Publishing.
6. Yamakita, R., Ishino, Y., Kato, M. and Ohiwa, N., An Investigation on Thermal Recycling of Recycled Plastic Resin (Optical Analysis of Abrupt Heating Characteristics of a Micro Plastic-Resin Particle), *Transactions of JSME*, (in Japanese), **72-716B**, 1060-1066 (2006).
  7. Yamakita, R., Ishino, Y. and Ohiwa, N., An Attempt at Numerical Prediction of Unburnt Rate in Recycled Plastic Resin Powder Combustion, *Proceedings of the 2nd International Symposium on Micro and Nano Technology*, 173-176 (2006).
  8. Yamakita, R., Ishino, Y. and Ohiwa, N., An Investigation on Thermal Recycling of Recycled Plastic Resin (Combustion Characteristics of PET-Resin Powder in a Ceramic Kiln Furnace), *Journal of Environment and Engineering*, **2-1**, 136-147 (2007).
  9. Ishino, Y., Yamakita, R. and Ohiwa, N., Appearances of Internal Micro Bubbling, Multiple Micro Explosions, Multiple Micro Jets and Micro Diffusion Flames around an Abruptly Heated Micro PET-Resin Particle, *Proceedings of the Combustion Institute*, **31**, 2097-2105 (2007).
  10. Yamakita, R., Ishino, Y., Kato, M. and Ohiwa, N., An Investigation on Thermal Recycling of Recycled Plastic Resin (Effects of Replacement Rate and Median Diameter of PET-Powder on In-Furnace Combustion), *Journal of Environment and Engineering*, **2-1**, 160-171 (2007).
  11. Ishino, Y., Yamakita, R. and Ohiwa N., High-Speed and Magnifying Observations of Ignition and Burning Processes of Micro PET Particles Flying through a Two-Dimensional Premixed Flame Front, *Proceedings of the 6th Pacific Symposium on Flow Visualization and Image Processing*, CD-ROM, Paper No. A2-1, (2007).
  12. Plastic Waste Management Institute of Japan ed., *Fundamental Data Book for Thermal Recycling of Plastic Resin*, (in Japanese), 27-59 (1993).
  13. JSTP ed., *Handbook of Polymer Processing*, (in Japanese), 2nd ed., 37 (2002), Nikkan Kogyo Press.
  14. Maruzen ed., *Handbook of High Polymer*, (in Japanese), 1015 (1994), Maruzen.
  15. AIST ed., *Data Base of Thermal Properties of Plastics*, <http://riodb.ibase.aist.go.jp/ptdb/entaruipi.htm>, National Institute of Advanced Industrial Science and Technology.
  16. Iwanami ed., *Physicochemical Handbook*, (in Japanese), 5th ed., 699, 975, 1275 (2005), Iwanami Publishing.
  17. Kobayashi, K., Investigation on Vaporization and Combustion of Droplets (3rd Report: Combustion), *Transactions of JSME*, (in Japanese), **20-100**, 837-843 (1954).
  18. Harris, M., E. Grumer J., von Elbe G. and Lewis B., Burning Velocities, Quenching, and Stability Data on Non-turbulent Flames of Methane and Propane with Oxygen and Nitrogen, *Proceedings of the Combustion Institute*, **3**, 80-89 (1949), Williams & Wilkins, Baltimore.
  19. Yamaoka, I. and Tsuji, H., Determination of Burning Velocity Using Counter-Flow Flames, *Proceedings of the Combustion Institute*, **20**, 1883-1892 (1985).